scientific reports

Check for updates

OPEN

Effects of coiling embolism on blood hemodynamic of the MCA aneurysm: a numerical study

Peiman Valipour

One of common endovascular technique for treatment of MCA aneurysm is using coiling gel for limiting of blood stream. In this work, computational fluid dynamic is used for the simulation of the blood hemodynamic inside MCA in existence of coiling gel. This work has tried to visualize the impacts of blood characteristics i.e. hematocrit as a protein related factor on efficiency of coiling fiber inside the aneurysm. Tufts of polyester fibers may be attached to the coil to support thrombosis and platelet aggregation. Blood rheology analysis is done by solving RANS equations and it is assumed that blood stream is non-Newtonian with fluid–solid interaction. OSI and WSS are compared on sac surface area for different stages of blood cycle. Achieved results confirm that the coiling gel substantially decreases the blood circulation inside the aneurysm sac. It is also found that the influence of blood hematocrit decreases when the MCA aneurysm is filled by the coiling gel.

One of the main source for the brain hemorrhage is the rupture of the cerebral aneurysm. Although this may cause fatal diseases on human, the exact source of aneurysm formation is not presented yet[1,2]. The formation and growth of the cerebral aneurysm is the mainly related to the blood rheology and characteristics. The early reports have shown that the blood flow features of Wall shear stress (WSS) and OSI have great impact on the rupture and bleeding of the cerebral aneurysms[3,4].

The advance in the computational techniques has enabled scientists to calculate this hemodynamics on the wall of the aneurysm[5,6]. Besides, technique of the magnetic resonance angiography (MRA) and computed tomography angiography (CTA) offer valuable information on the shape and feature of the real three-dimensional aneurysm which is essential for the computational modeling. In fact, analysis of the real geometry offers more reliable information about the aneurysm growth and rupture[7–9].

Although presented results by different scholars are not consistent, there are some identical outcomes and analysis that define the main potential risks related to aneurysm rupture[10,11]. Too overcome these inconsistence, several indices and factors have presented and investigated in recent years[12,13]. The medical phenotype and evolution of aneurysms are not the same, and heterogeneity is noticed. Previous studies showed that transparent, small, type I aneurysms evolved swiftly, while a long time is required for the expansion of type II, thick-walled aneurysms[14–16]. Moreover, more inflammatory permeation in the pathological samples of type II aneurysms are available than those of type I aneurysms.

Aneurysm rupture and growth have two independent haemodynamic corridors: in first one, a positive WSS gradient and a high WSS prompt the cell-mediated formation of a small, thin-walled, translucent aneurysm; in another way, high OSI and a low WSS prompt the expression of inflammatory elements that mediate the formation of a thick-walled, atherosclerotic aneurysm[17,18]. Nevertheless, large-scale clinical experimental evidence did not support this hypothesis. Comprehensive literature survey on estimating rupture risk, growth, and endovascular device assessment indicates that WSS and OSI are the main hemodynamic factors have great impacts[19,20].

One of the most common endovascular technique for treatment of the cerebral saccular aneurysm is coiling technique in which the main portion of the sac are filled with gel (Fig. 1). Shape memory polymers (SMPs) are materials with unlimited potential for this application, because of their versatile and tunable shape memory properties that can be tailored to a patient's aneurysm geometry and flow condition. Simple coiling denotes to the transfer and packing of detachable coils within the aneurysmal sac via a microcatheter into the aneurysmal dome. The existence of the coil would dense packing and induce rapid blood accumulation formation within the aneurysmal sac, and consequently, sac is separated from the main flow stream. This technique is useful for most of IAs with dome-to-neck ratios (> 2.0). Although several computational studies have done for analysis of blood hemodynamic within cerebral aneurysms, evaluation of the hemodynamic effects of the coiling technique

Department of Textile Engineering, Clothing and Fashion, Qaemshahr Branch, Islamic Azad University, Qaemshahr, Iran. email: pe.valipour@iau.ac.ir

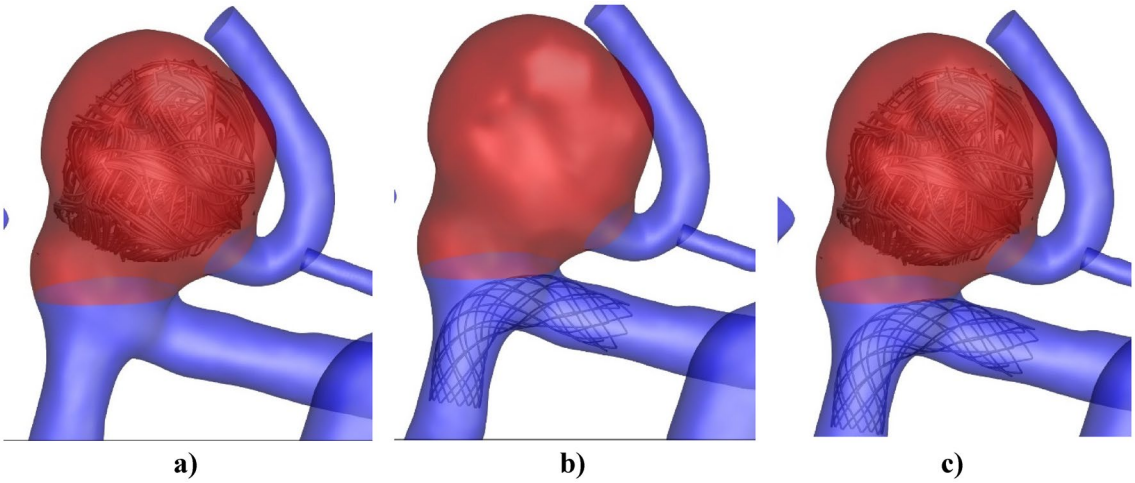

Figure 1. MCA aneurysm with (**a**) coiling (**b**) fiber-based stents stent (**c**) coiling and stent.

inside MCA aneurysm was not fully investigated in existence articles[21–25]. In this work, blood rheology effects inside the MCA aneurysm with/without coiling are fully investigated.

Drug Eluting Stent (DES) is the Second Generation of Vascular Stent. To solve the problem of In-Stent Restenosis, the bare metal stent as the structural basis is recommended by the researchers and coated it with the biocompatibility coating and anti-proliferative drugs lastly advanced the second-group stent—drug-eluting stent (DES), which means non-absorbable or bioabsorbable polymers or polymer-free stents. The features of stents are altered because of adding polymers, e.g., biomechanics and biocompatibility.

In the present research, computational technique of CFD is applied for the modeling of non-Newtonian, transient blood flow inside real MCA aneurysm. WSS and OSI factors are compared and evaluated in different stages of blood cycle. Influence of blood hematocrit is also investigated on hemodynamic factors.

Problem description and computational methods

It is confirming that all methods were carried out in accordance with relevant guidelines and regulations. Besides, all experimental protocols were approved by of the Ca' Granda Niguarda Hospital and it is confirmed that informed consent was obtained from all subjects and/or their legal guardian(s).

The selected MCA aneurysm is demonstrated in Fig. 2. The geometry of this aneurysm is obtained from Aneurisk webpage[26]. The main reason for selection of this aneurysm is its dome-to-neck ratios which is more than 2.0 and coiling technique is used for the treatment of this aneurysm.

The simulation of bloodstream is done by using simple algorithm with one-way FSI model[27–30]. In this technique, the force from blood stream is applied as exterior force on the structure of the vessel wall[31–33]. Blood stream is assumed non-Newtonian, viscoelastic and transient. The applied boundary condition for inlet is mass flow rate while outlet pressure is applied at outlet of the domain. Figure 3a and 3b demonstrate the applied mass flow rate at inlet and pressure at outlet of domain, respectively. The time step of our simulations is 2 ms. The range of hematocrit is 0.4 to 0.5 in which male hematocrit range is 0.4–0.53. For the estimation of the blood viscosity, Casson model is used since this model calculates the viscosity based on the hematocrit value[34].

For modeling of coiling, the whole domain inside the sac section is assumed porous media and effects of different coiling fractions are applied via changing the permeability of the porous region as presented in Table 1. In this technique, the porous media is estimated as a layer of solid material with straight parallel pipes of a permanent cross-sectional figure intersecting sample[35].

The produced grid is demonstrated in Fig. 4. The resolution of the generated grid near the aneurysm and vessel wall is higher than other sections since the calculation of the hemodynamic factor should be done with higher precision. Grid study is also performed to find possible relationship between obtained results and size of produced grids. Table 2 present more details about generated grid and results of average WSS for produced grids are compared. The presented results are related to model at peak systolic stage (m = 6.8 mg/s) with HCT = 0.4. It is found that model 3rd with 919,953 cells (with element size of 0.2) is a good option for our investigations.

Results and discussion

The variation of the WSS on the sac wall in different stages of blood cycle are demonstrated in Fig. 5. In these contours, the porosity of coiling is not applied. As expected, maximum value of WSS initiated at peak systolic stage (t = 0.24 s) and remains in the maximum deceleration (t = 0.36) stage. The contour of pressure on the sac surface is illustrated in Fig. 6 and maximum pressure is noticed in the dome of the aneurysm. Comparison of the blood iso-surface in different stage clearly illustrates the blood hemodynamic in various stages of blood cycle (Fig. 7).

The influence of the hematocrit on WSS is demonstrated in Fig. 8 at peak systolic stage (t = 0.24 s). The contour shows that increasing blood HCT would increases the WSS near ostium section while WSS near the dome remains unchanged. This is mainly because of the high velocity of the blood stream near the ostium section.

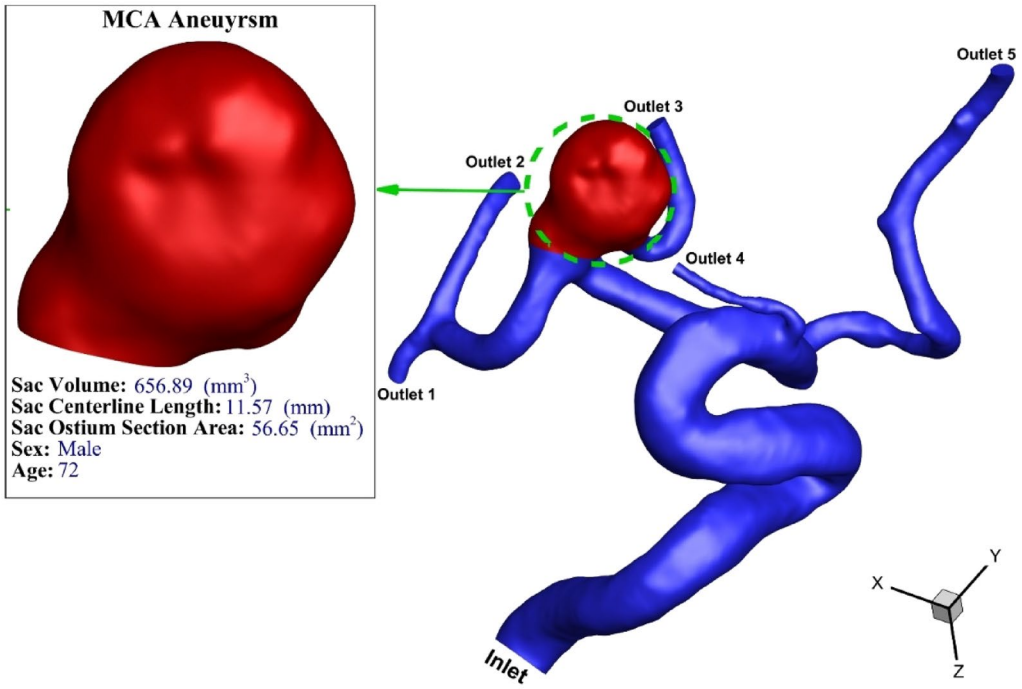

Figure 2. Geometry of chosen MCA aneurysm.

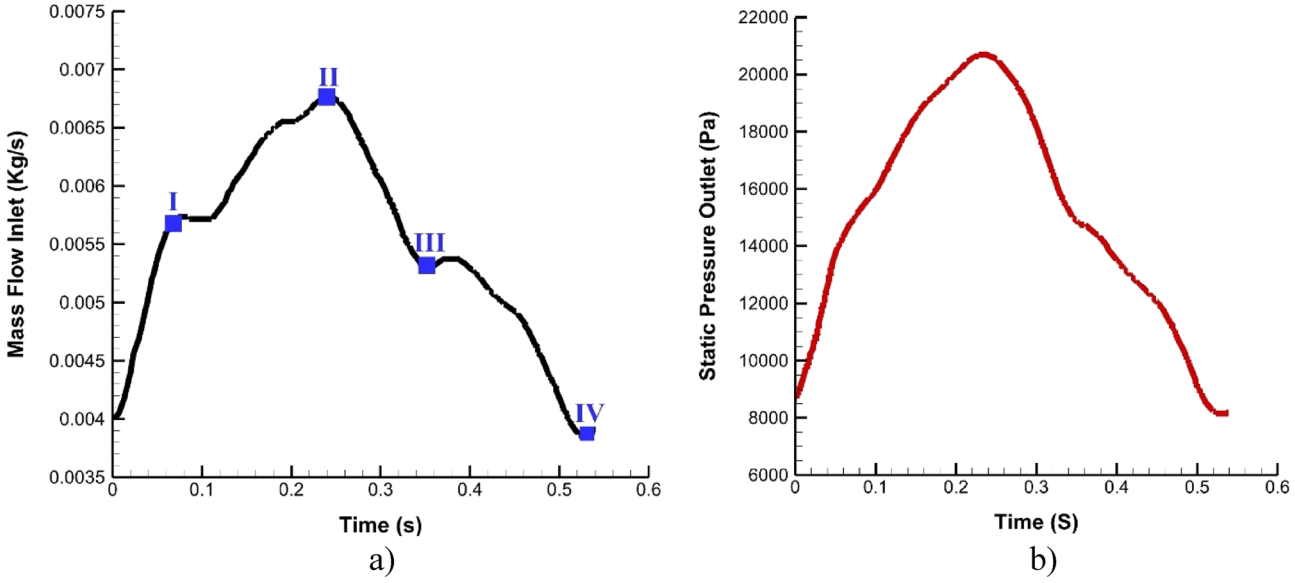

Figure 3. Applied boundary condition at inlets and outlets.

Porosity	L Coil(m)	d Coil (m)	s Coil (m2)	v-Aneurysm (m3)	Inter sur area (1/m)	Prem (m2)	1/Prem
0.75	0.3	2.5 E−04	2.39E−04	7.06E−07	3.38E+02	1.83E−06	5.44E+05
0.85	0.3	2.5 E−04	2.39E−04	7.06E−07	3.38E+02	2.67E−06	3.74E+05

Table 1. Details of applied coiling for selected MCA aneurysm.

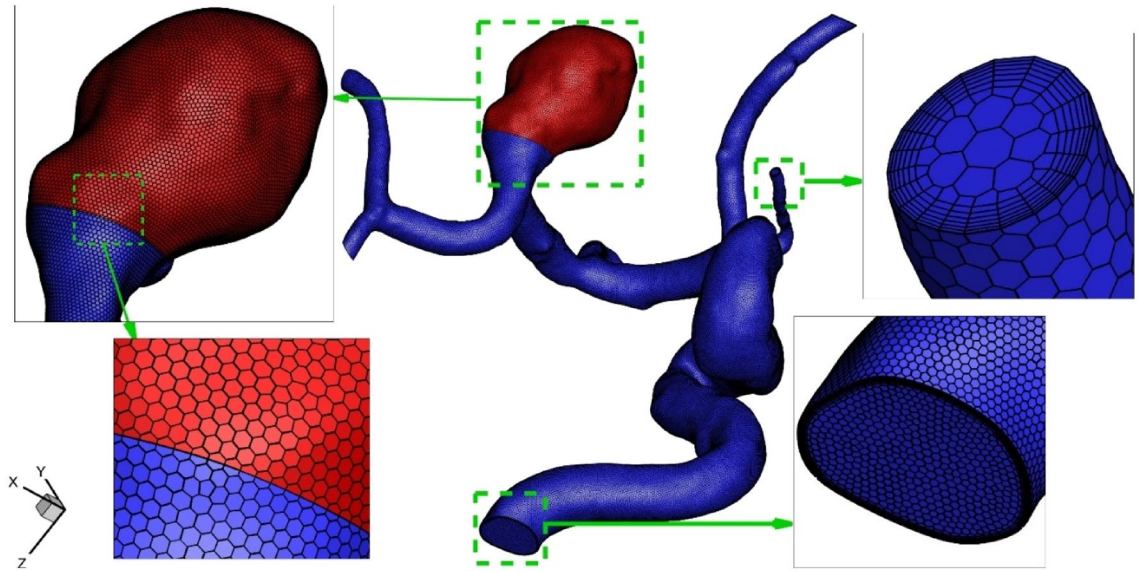

Figure 4. Applied grid for our model.

	Element-size	Number of elements	Ave WSS on Sac (Pa)	Change %
Coarse	0.30	448,379	2	–
Medium	0.25	654,791	2.8	40
Fine	0.20	919,953	3.52	25
Very fine	0.15	1,356,897	3.58	2

Table 2. Details of used grids.

The influence of the coiling porosity on the distribution of the WSS are demonstrated in Fig. 9. Due to importance of this factor, the variations of this factor are displayed in two sides in this figure. Presented results confirm that the critical region with high WSS happens near the sac ostium section. The variations of the shear stress also defined that the dome of the sac section is less important in the selected model. Previous research shows that the rupture of the aneurysm is more happens in a positive WSS gradient and a high WSS. Thus, ostium section has potential for the rupture. The results of pressure distribution for different porosity values (Fig. 10) also confirm that pressure gradient near sac ostium is higher than other regions at peak systolic.

Quantitative comparison of the maximum AWSS on sac surface (Fig. 11) demonstrates that increasing the hematocrit rises the maximum WSS on sac surface. Effects of the porosity values has limited impact on this factor. The variation of OSI value calculated at the end of the 3rd cycle is demonstrated in Fig. 12. Achieved results confirm that the effect of the hematocrit (HCT) on the cases with coiling is limited. Meanwhile, decreasing the porosity increases the permeability which means that more domain is filled with coils. Hence, OSI index significantly reduces when aneurysm is filled by coiling gel.

Conclusion

In present work, the impacts of the coiling on hemodynamic of the blood stream inside MCA aneurysm are investigated. The effect of endovascular coiling is applied by filling the sac section area with porous media. The influences of blood hematocrit value on the distribution of WSS on the sac surface is fully explained. Comparison of the OSI value for different coiling porosities are done to disclose the influence of the coiling technique on the reduction of aneurysm rupture risk. Computational technique of CFD is used for the visualization of the blood flow inside the MCA aneurysm. Our results show that the usage of the coiling considerably reduces the WSS since blood stream circulation is limited in the sac section area. Meanwhile, the blood hematocrit effects are limited by usage of coiling inside the sac region.

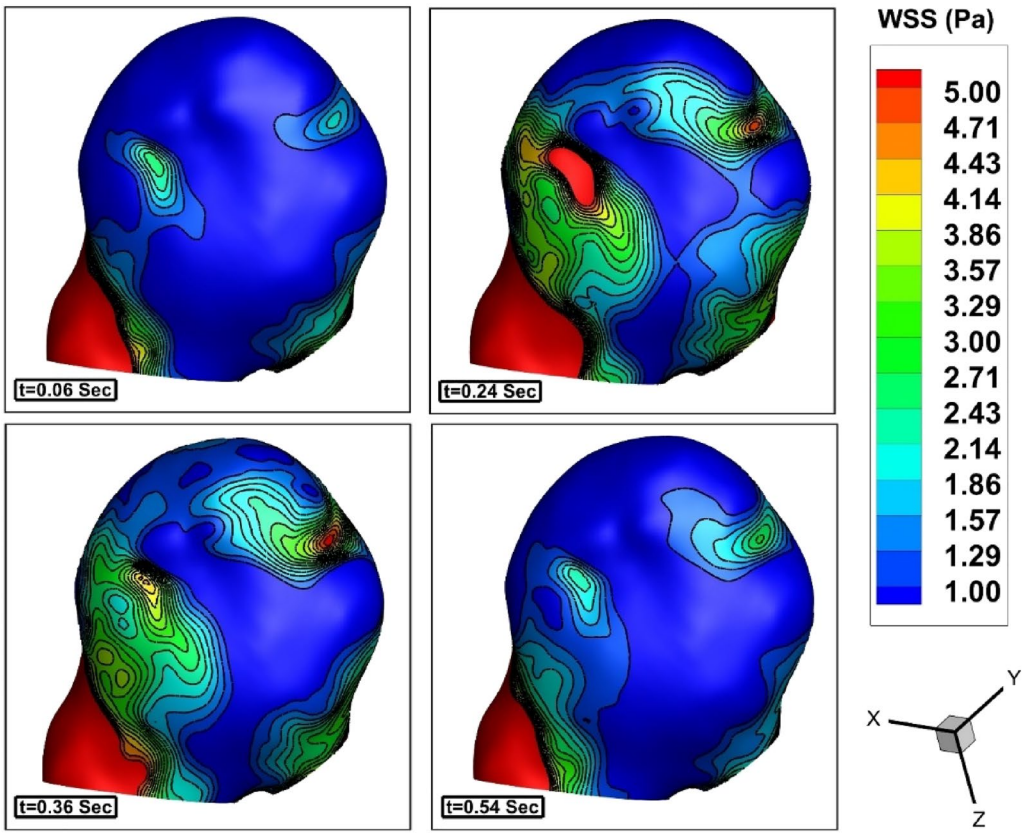

Figure 5. Variation of the WSS on the sac wall in different stages of blood cycle.

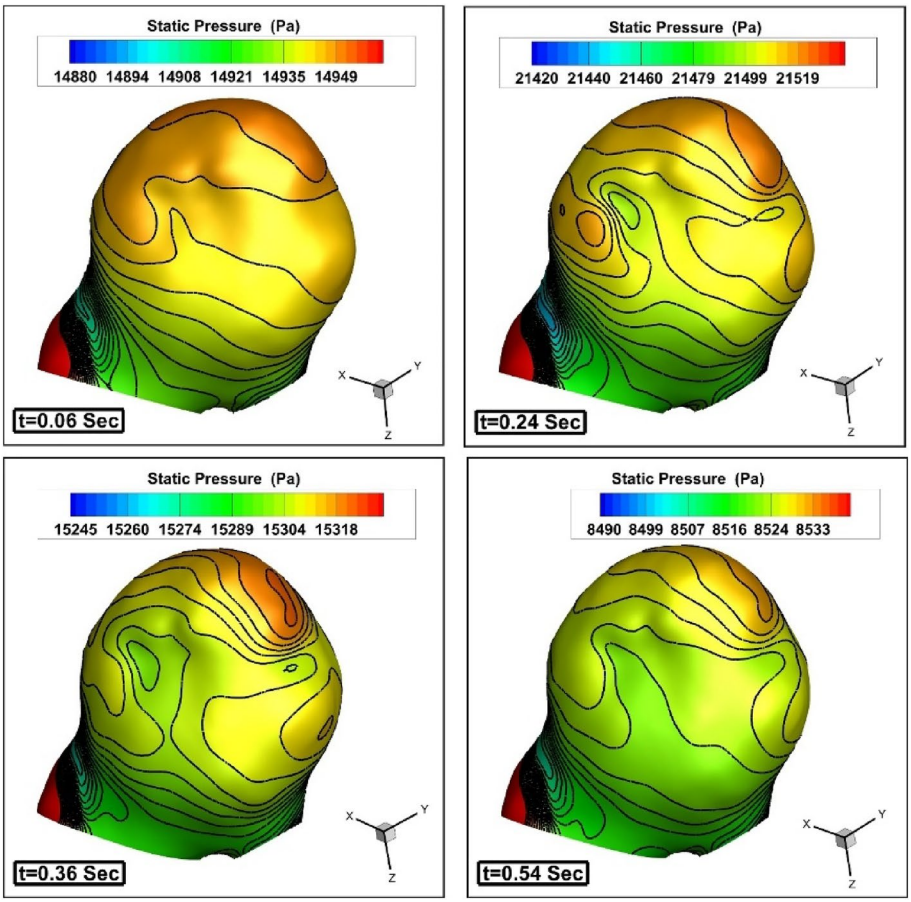

Figure 6. Pressure contour on the sac surface (without coiling).

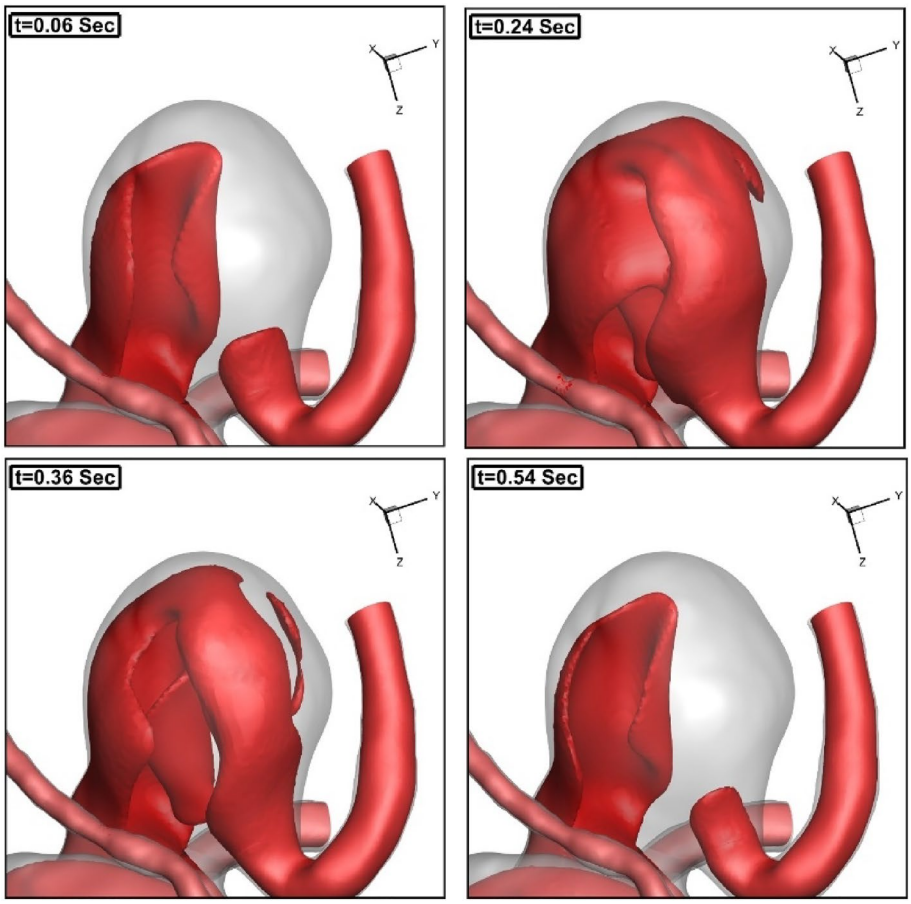

Figure 7. Comparison of is-velocity surface in different stages.

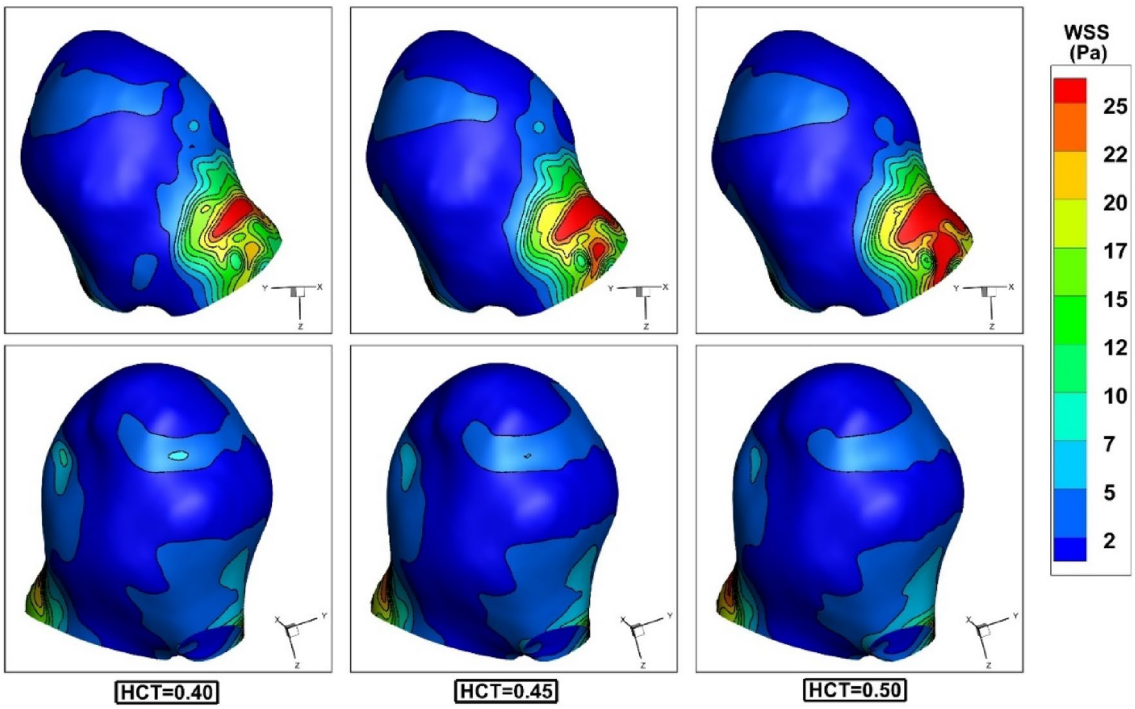

Figure 8. Effects of hematocrit on the WSS distribution at peak systolic.

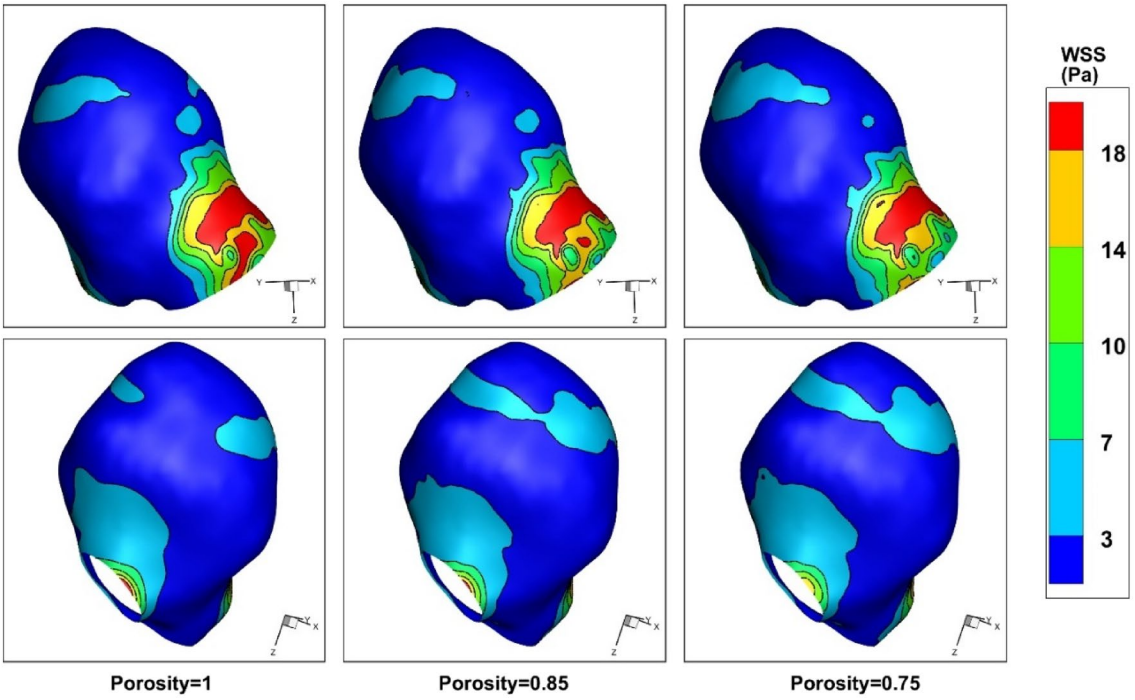

Figure 9. Effects of coiling porosity on WSS at peak systolic.

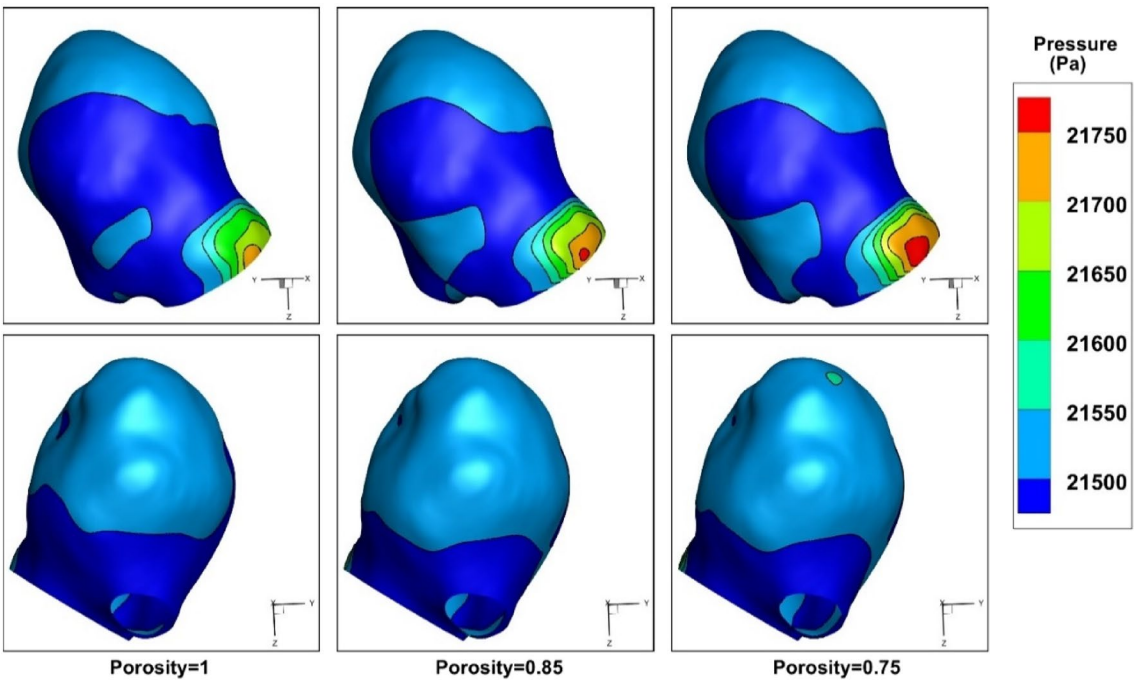

Figure 10. Effects of coiling porosity on pressure distribution at peak systolic.

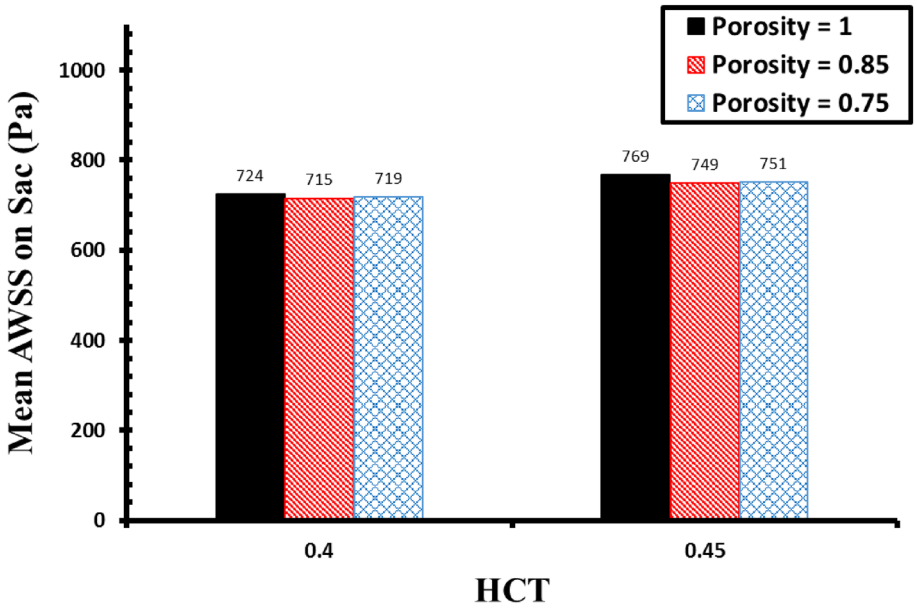

Figure 11. Impacts of HCT and coiling porosity on Mean AWSS on sac surface.

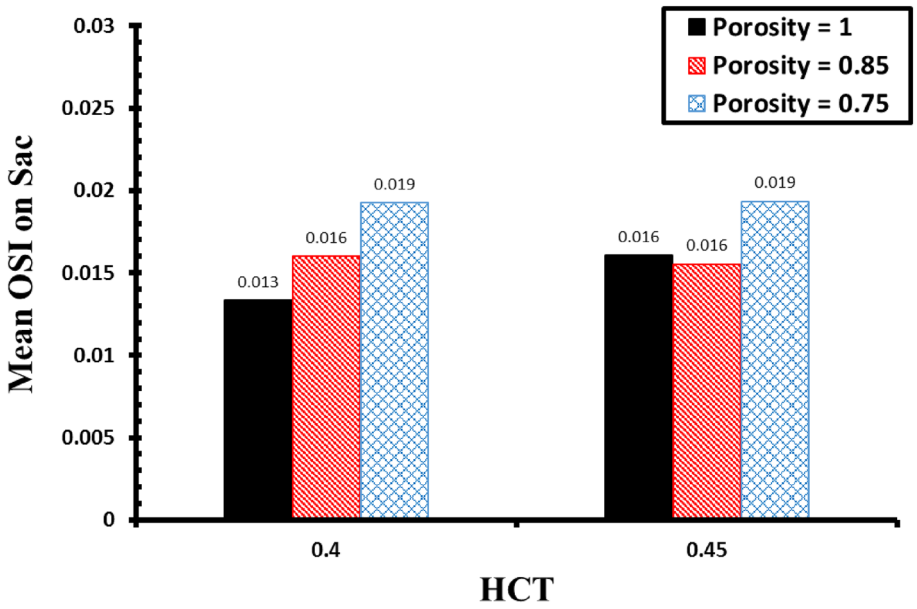

Figure 12. Impacts of HCT and coiling porosity on OSI at end of blood cycle (t = 0.54 s).

Data availability

All data generated or analysed during this study are included in this published article.

Received: 1 November 2022; Accepted: 12 December 2022
Published online: 20 December 2022

References

1. Jin, Z.-H., Gerdroodbary, M. B., Valipour, P., Faraji, M. & Abu-Hamdeh, N. H. CFD investigations of the blood hemodynamic inside internal cerebral aneurysm (ICA) in the existence of coiling embolism. *Alex. Eng. J.* https://doi.org/10.1016/j.aej.2022.10.070 (2023).
2. Sadeh, A., Kazemi, A., Moharam BahramKhoo, M. & Gerdroodbary, B. Computational analysis of the blood hemodynamic inside internal cerebral aneurysm in the existence of endovascular coiling. *Int. J Mod. Phys. C* https://doi.org/10.1142/S0129183123500596 (2023).

3. Dai, J. *et al.* Electrochemical degradation of antibiotic enoxacin using a novel PbO_2 electrode with a graphene nanoplatelets interlayer: Characteristics, efficiency and mechanism. *Chemosphere* **307**, 135833. https://doi.org/10.1016/j.chemosphere.2022.135833 (2022).
4. Rostamian, A., Fallah, K., Rostamiyan, Y. & Alinejad, J. Application of computational fluid dynamics for detection of high risk region in middle cerebral artery (MCA) aneurysm. *Int. J. Mod. Phys. C* https://doi.org/10.1142/S0129183123500195 (2022).
5. Sheidani, A. *et al.* Influence of the coiling porosity on the risk reduction of the cerebral aneurysm rupture: Computational study. *Sci. Rep.* https://doi.org/10.1038/s41598-022-23745-1 (2022).
6. Shen, X.-Y., Gerdroodbary, M. B., Poozesh, A., Musa Abazari, A. & Imani, S. M. Effects of blood flow characteristics on rupture of cerebral aneurysm: Computational study. *Int. J. Mod. Phys. C* **32**(11), 2150143 (2021).
7. Liu, C. *et al.* Engineered extracellular vesicles and their mimetics for cancer immunotherapy. *J. Control. Release* **349**, 679–698. https://doi.org/10.1016/j.jconrel.2022.05.062 (2022).
8. Hoi, Y. *et al.* Effects of arterial geometry on aneurysm growth: Three-dimensional computational fluid dynamics study. *J. Neurosurg.* **101**, 676–681 (2004).
9. Li, Z. *et al.* Sb-doped WO.sub.3 based QCM humidity sensor with self-recovery ability for real-time monitoring of respiration and wound. *Sens. Actuators B Chem.* **361**, 131691. https://doi.org/10.1016/j.snb.2022.131691 (2022).
10. Yang, W., Liu, W., Li, X., Yan, J. & He, W. Turning chiral peptides into a racemic supraparticle to induce the self-degradation of MDM2. *J. Adv. Res.* https://doi.org/10.1016/j.jare.2022.05.009 (2022).
11. Tateshima, S. *et al.* Three-dimensional blood flow analysis in a wide necked internal carotid artery-ophthalmic artery aneurysm. *J. Neurosurg.* **99**, 526–33 (2003).
12. Hao, P. *et al.* Serum metal ion-induced cross-linking of photoelectrochemical peptides and circulating proteins for evaluating cardiac ischemia/reperfusion. *ACS Sensors* **7**(3), 775–783. https://doi.org/10.1021/acssensors.1c02305 (2022).
13. Steinman, D. A., Milner, J. S., Norley, C. J., Lownie, S. P. & Holdsworth, D. W. Image-based computational simulation of flow dynamics in a giant intracranial aneurysm. *Am. J. Neuroradiol.* **24**, 559–566 (2003).
14. Chatziprodromou, I., Butty, V., Makhijani, V. B., Poulikakos, D. & Ventikos, Y. Pulsatile blood flow in anatomically accurate vessels with multiple aneurysms: A medical intervention planning application of computational haemodynamics. *Flow Turbul. Combust.* **71**, 333–346 (2003).
15. Shen, X.-Y., Gerdroodbary, M. B., Abazari, A. M. & Moradi, R. Computational study of blood flow characteristics on formation of the aneurysm in internal carotid artery. *Eur. Phys. J. Plus.* **136**(5), 541 (2021).
16. Shen, X.-Y. *et al.* Numerical simulation of blood flow effects on rupture of aneurysm in middle cerebral artery. *Int. J. Mod. Phys. C* **33**(03), 2250030 (2022).
17. Fung, Y. C. *Biomechanics: Mechanical properties of living tissues* 2nd edn. (Springer, 1993).
18. Razavi, A., Shirani, E. & Sadeghi, M. Numerical simulation of blood pulsatile flow in a stenosed carotid artery using different rheological models. *J Biomech.* **44**, 2021–2030 (2011).
19. Misagh Imani, S. *et al.* Application of finite element method to comparing the NIR stent with the multi-link stent for narrowings in coronary arteries. *Acta Mech. Solida Sin.* **28**(5), 605–612 (2015).
20. Malvè, M. *et al.* Impedance-based outflow boundary conditions for human carotid haemodynamics. *Comput. Methods Biomech. Biomed. Engin.* **17**(11), 1248–1260 (2014).
21. Feng, Y. *et al.* Pan-cancer analysis and experiments with cell lines reveal that the slightly elevated expression of DLGAP5 is involved in clear cell renal cell carcinoma progression. *Life Sci.* **287**, 120056. https://doi.org/10.1016/j.lfs.2021.120056 (2021).
22. Wang, H. *et al.* Transcranial alternating current stimulation for treating depression: A randomized controlled trial. *Brain* **145**(1), 83–91. https://doi.org/10.1093/brain/awab252 (2022).
23. Lai, W. & Wong, W. Property-tuneable microgels fabricated by using flow-focusing microfluidic geometry for bioactive agent delivery. *Pharmaceutics* **13**(6), 787. https://doi.org/10.3390/pharmaceutics13060787 (2021).
24. Lai, W. Development of hydrogels with self-healing properties for delivery of bioactive agents. *Mol. Pharm.* **18**(5), 1833–1841. https://doi.org/10.1021/acs.molpharmaceut.0c00874 (2021).
25. Lai, W. Non-conjugated polymers with intrinsic luminescence for drug delivery. *J. Drug Deliv. Sci. Technol.* **59**, 101916. https://doi.org/10.1016/j.jddst.2020.101916 (2020).
26. AneuriskWeb project website, http://ecm2.mathcs.emory.edu/aneuriskweb. Emory University, Department of Math&CS, 2012.
27. Isanejad, M. & Fallah, K. Numerical study of droplet breakup in an asymmetric T-junction microchannel with different cross-section ratios. *Int. J. Mod. Phys. C* **33**(02), 2250023 (2022).
28. Fallah, K. & Fattahi, E. Splitting of droplet with different sizes inside a symmetric T-junction microchannel using an electric field. *Sci. Rep.* **12**(1), 1–12 (2022).
29. Allahyari, S. *et al.* Investigating the effects of nanoparticles mean diameter on laminar mixed convection of a nanofluid through an inclined tube with circumferentially nonuniform heat flux. *J. Eng. Thermophys.* **25**(4), 563–575 (2016).
30. Fallah, K., Rahni, M. T., Mohammadzadeh, A. & Najafi, M. Drop formation in cross-junction microchannel, using lattice Boltzmann method. *Therm. Sci.* **22**(2), 909–919 (2018).
31. Sadeghi, A., Amini, Y., Saidi, M. H. & Yavari, H. Shear-rate-dependent rheology effects on mass transport and surface reactions in biomicrofluidic devices. *AIChE J.* **61**(6), 1912–1924 (2015).
32. Heydari, A., Alborzi, Z. S., Amini, Y. & Hassanvand, A. Configuration optimization of a renewable hybrid system including biogas generator, photovoltaic panel and wind turbine: Particle swarm optimization and genetic algorithms. *Int. J. Mod. Phys. C* https://doi.org/10.1142/S0129183123500699 (2022).
33. Sadeghi, A., Amini, Y., Saidi, M. H. & Chakraborty, S. Numerical modeling of surface reaction kinetics in electrokinetically actuated microfluidic devices. *Anal. Chim. Acta* **838**, 64–75 (2014).
34. Boccadifuoco, A., Mariotti, A., Celi, S., Martini, N. & Salvetti, M. V. Impact of uncertainties in outflow boundary conditions on the predictions of hemodynamic simulations of ascending thoracic aortic aneurysms. *Comput. Fluids* **165**, 96–115 (2018).
35. Mitsos, A. P., Kakalis, N. M., Ventikos, Y. P. & Byrne, J. V. Haemodynamic simulation of aneurysm coiling in an anatomically accurate computational fluid dynamics model. *Neuroradiology* **50**(4), 341–347 (2008).

Author contributions

P.V. wrote the main manuscript text and prepared figures.

Competing interests

The author declares no competing interests.

Additional information

Correspondence and requests for materials should be addressed to P.V.

Reprints and permissions information is available at www.nature.com/reprints.